Computers & Geosciences 49 (2012) 190–199

Contents lists available at SciVerse ScienceDirect

Computers & Geosciences

journal homepage: www.elsevier.com/locate/cageo

Load Love numbers and Green's functions for elastic Earth models PREM, iasp91, ak135, and modified models with refined crustal structure from Crust 2.0☆

Hansheng Wang [a,*], Longwei Xiang [a,b], Lulu Jia [a,b], Liming Jiang [a], Zhiyong Wang [c], Bo Hu [a,b], Peng Gao [a,b]

[a] State Key Laboratory of Geodesy and Earth's Dynamics, Institute of Geodesy and Geophysics, Chinese Academy of Sciences, Wuhan 430077, China
[b] Graduate University of Chinese Academy of Sciences, Beijing 100049, China
[c] Department of Surveying Engineering, Shandong University of Technology, Zibo 255049, China

ARTICLE INFO

Article history:
Received 29 October 2011
Received in revised form
26 June 2012
Accepted 27 June 2012
Available online 7 July 2012

Keywords:
Loading Love numbers
Green's function
PREM
iasp91 and ak135
Crust 2.0

ABSTRACT

Load Love numbers and Green's functions are computed for elastic Earth models PREM, iasp91 and ak135, and their modified models with refined crustal structure from Crust 2.0. It is found that the differences of results between iasp91 or ak135 and PREM, and the effects of refinement of crustal structure are significant for the Love numbers of degrees from around 200 to very high numbers, and for the Green's functions in the near-field. The results of the models given in this paper are applicable to the studies related to loading processes (present surface mass transport as measured by GRACE and GPS, ocean tide loading, etc.), making it possible to use different models or assess the uncertainties of solutions of the loading problems under investigation. In order to ensure the stability of the solutions for degrees larger than 360 (or when the resolution is less than 55 km), a variable transformation on the solution vector is used in this paper and proved to work effectively.

1. Introduction

Since both load Love numbers (LLNs) and load Green's functions (LGFs) are dependent strongly upon the *P*-wave velocity V_P, *S*-wave velocity V_S and density ρ for a spherically-symmetric non-rotating elastic isotropic (SNREI) Earth model, the numerical results must be updated along with the development of new Earth models with new data constraints.

PREM Earth model (Dziewonski and Anderson, 1981) used the data of body wave travel times and the periods of normal modes from years 1964 to 1975 collected by the International Seismological Centre (ISC). For Earth model iasp91 (Kennett and Engdahl, 1991), the data of body waves used were extended to 1987 and for the follow-on ak135 model (Kennett et al., 1995), the data of *P* wave were extended to 1991. The largest differences of elastic structures between iasp91/ak135 and PREM can be found in the shallow part of the Earth (Figs. 1 and 2). Especially, PREM includes a discontinuity at depth 220 km which iasp91 and ak135 do not support. The differences between model iasp91 and ak135 are usually very small except for the *S*-wave velocity within 50 km depth. However, although the subsequent Earth models iasp91 and ak135 were already produced, the model PREM has been widely used to investigate the loading responses to ocean tide, terrestrial water change, ice-melting, and last deglaciation since it was proposed in 1981 (e.g., Han and Wahr, 1995; Wang et al., 1996; Guo et al., 2001; Van Dam et al., 2002). In spite of the changes of elastic structures of the two new models compared with PREM, they have been neglected for a long time in loading process modeling. Recently, Na and Baek (2011) presented the results of LNNs and LGFs for iasp91 model. However, the highest degree is limited to 10,000.

Moreover, although Crust 2.0 (Laske et al., 2012) has been producing new results of crustal elastic structure with increasing resolution in depth direction, showing large gaps in comparison with the above three models (Fig. 2), it has usually not been included in the Earth model for the modeling of loading process.

Accordingly, the aim of this paper is to compute the LLNs and LGFs for the three representative Earth models and the modified models with crust substituted by the globally-averaged Crust 2.0, and to investigate how the differences in Earth's elastic structures affect the numerical results.

For the computation of LLNs and LGFs, some previous works have been taken into account the lateral heterogeneity (e.g., Plag et al., 1996) and the anisotropy of mantle (e.g., Pagiatakis, 1990) which are, however, not the topics of this paper.

2. Numerical method

LGF is defined as the surface deformation of the Earth due to a point load on the Earth's surface (Longman, 1962, 1963), and can

☆The data is available from server at http://www.iamg.org/CGEditor/index.htm.

* Corresponding author. Tel.: +86 276881341; fax: +86 278673841.
E-mail address: whs@asch.whigg.ac.cn (H. Wang).

0098-3004/$ - see front matter © 2012 Elsevier Ltd. All rights reserved.
http://dx.doi.org/10.1016/j.cageo.2012.06.022

be conveniently expressed through three LLNs (h_n, l_n, k_n) (Farrell, 1972). For an arbitrarily distributed mass load on the surface, the resultant responses can be computed by convoluting the related LGFs and the load (Peltier and Andrews, 1976; Wu and Peltier, 1982). Thus, in this paper we focus on the computation of LLNs and LGFs for the Earth models mentioned above. The fundamental methodology related to the computations can be found in previous works (e.g., Longman, 1962; Farrell, 1972; Wu and Peltier, 1982). As in Wu and Peltier (1982), one can find how the partial differential field equations are transformed into ordinary differential equations (ODEs, Eq. (8)), and how the ODEs are solved by the Runge–Kutta method using boundary conditions at the core–mantle boundary (CMB) (Eq. (48)) and on the Earth's surface (Eq. (11)), then we compute the LLNs (Eq. (12)) and LGFs (Farell, 1972) as also outlined in Appendix A and Appendix B. However, for higher degrees, the computation can be subjected to numerical overflow or instability. In order to ensure the stability when solving the ODEs for higher degrees, Riva and Vermeersen (2002) developed an approximate approach and Wang et al. (1996) proposed a variable transformation approach. In this paper, we use the latter one since it is not based on any assumption. It is noted that Wang et al. (1996) just mentioned the transformation of the ODEs but did not give the results transformed for the boundary conditions at CMB and on the Earth's surface, and the final formulas for LLNs. Therefore, in the following, we thoroughly formulate the related procedures for the transformation approach.

Since for an incompressible homogeneous SNREI model, as in Wu and Peltier (1982), the solution vector $Y=(y_1, y_2, y_3, y_4, y_5, y_6)^T$ of the ODEs (Eq. (8)) was found to have a r^n factor (e.g., Eq. (30)), for a compressible layered SNREI model considered in this paper, thus we can define a new solution vector Z transformed from Y in the following:

$$Y = r^n Z. \tag{1}$$

The numerical computation of Z would not overflow and would be stable. Inserting Eq. (1) into the ODEs (Eq. (8)) and surface boundary condition (Eq. (11)), we have new ODEs

$$\frac{dZ}{dr} = \left(A - \frac{n}{r}E\right)Z, \tag{2}$$

and new surface boundary condition,

$$\begin{cases} z_3(a) = r^{-n} y_3(a) \\ z_4(a) = r^{-n} y_4(a) \\ z_6(a) = r^{-n} y_6(a) \end{cases}, \tag{3}$$

where E is the unit matrix, and $[y_3(a), y_4(a), y_6(a)]$ are given by surface boundary condition (Eq. (11)). Since the same factor is used for the transformation of all the elements of the solution vector, the boundary condition at the CMB (Eq. (48)) is unchanged. However the solution (Eq. (49)) on the surface of a small uniform sphere ($r=\delta r$) located at the center of the core is transformed into $[1, 2(n-1)\delta r^{-1}]^T$ as initial value for integrating ODEs in the core (Eq. (8)).

Using the new solution vector Z, the corresponding LLNs computed as in Eqs. (A1) for $n>1$ can be written as:

$$\begin{bmatrix} h_n \\ l_n \\ k_n+1 \end{bmatrix} = \frac{g_0(a)}{\Phi_{2n}(a)} \begin{bmatrix} z_{11}(a) & z_{12}(a) & z_{13}(a) \\ z_{21}(a) & z_{22}(a) & z_{23}(a) \\ -z_{51}(a)/g_0 & -z_{52}(a)/g_0 & -z_{53}(a)/g_0 \end{bmatrix}$$

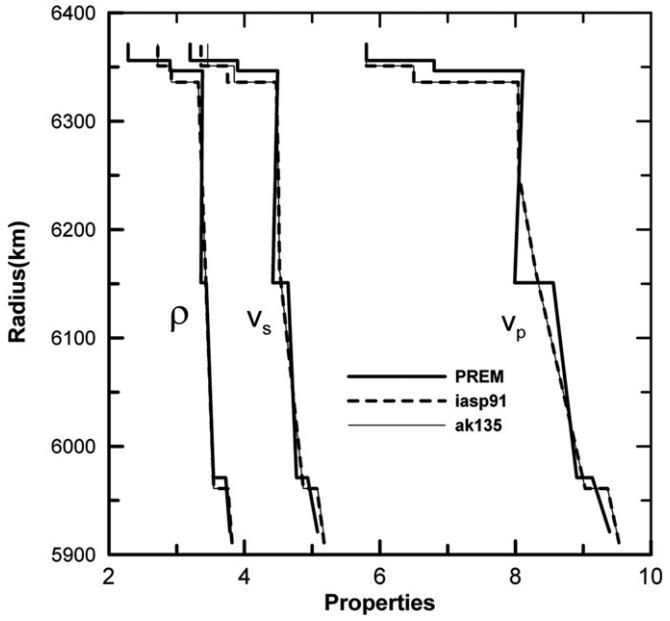

Fig. 1. Comparison of the density and velocity within 400 km depth among PREM, iasp91, and ak135. ρ—density; V_P—P-wave velocity and V_S–S-wave velocity.

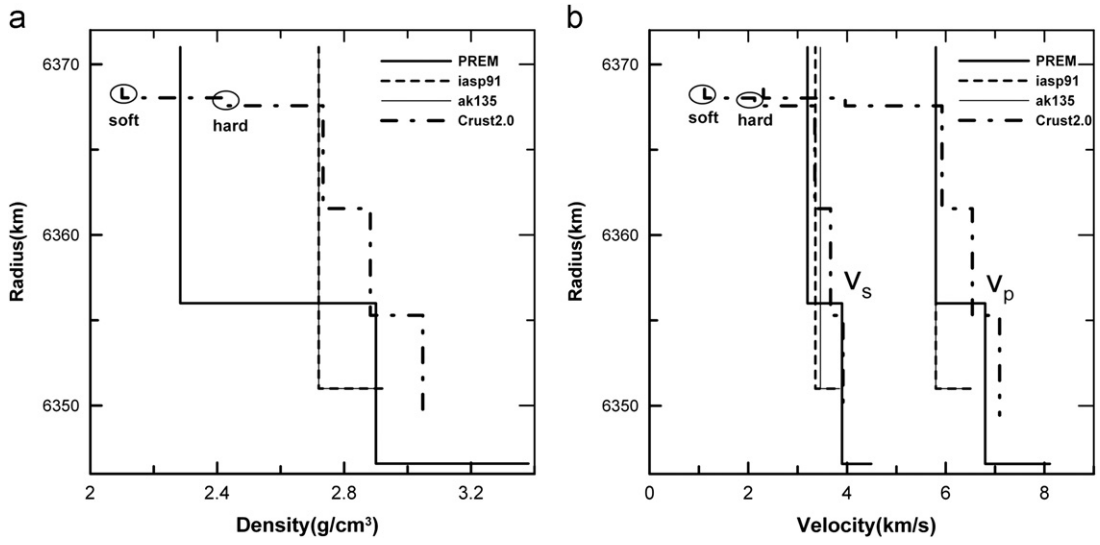

Fig. 2. Comparison of the density (a) and velocity (b) within 20 km depth among PREM, iasp91, ak135 and globally-averaged Crust 2.0. Soft/hard denotes soft/hard sediment with thicknesses of 0.52 km/0.46 km.

$$\times \begin{bmatrix} z_{31}(a) & z_{32}(a) & z_{33}(a) \\ z_{41}(a) & z_{42}(a) & z_{43}(a) \\ z_{61}(a) & z_{62}(a) & z_{63}(a) \end{bmatrix}^{-1} \begin{bmatrix} y_3(a) \\ y_4(a) \\ y_6(a) \end{bmatrix}, \quad n>1, \tag{4}$$

and the degree one LLNs for CE coordinate system (Farrell, 1972) can be calculated by (A.2) with

$$\begin{bmatrix} h_1^c \\ l_1^c \\ k_1^c+1 \end{bmatrix} = \frac{g_0(a)}{\Phi_{21}(a)} \begin{bmatrix} z_{11}(a) & z_{12}(a) \\ z_{21}(a) & z_{22}(a) \\ -z_{51}(a)/g_0 & -z_{52}(a)/g_0 \end{bmatrix} \times \begin{bmatrix} z_{31}(a) & z_{32}(a) \\ z_{41}(a) & z_{42}(a) \end{bmatrix}^{-1} \begin{bmatrix} y_3(a) \\ y_4(a) \end{bmatrix}, , \tag{5}$$

in which $\Phi_{2n}(a)=ag_0(a)/m_e$ is the coefficient of Legendre polynomial expansion for the potential of a surface unit mass load applied at the north pole, a is the Earth's radius, g_0 is the surface gravity and m_e is the total mass of the Earth. Eq. (5) is the basic LLNs for $n=1$ which can be used to give the results for different coordinate systems (see Appendix A, Table 1).

For the computation of LGFs, it is important to use efficient techniques for fast converging. It has been illustrated that the Kummer's transformation (Farrell, 1972) takes a very good effect when the LLNs have to be available for high degrees (e.g., Wang and Wang, 2007). In addition, the use of disk factor (Farrell, 1972) will improve the accuracy of the results in the far field. Therefore, in this paper Kummer's transformation together with the disk factor method is employed. Expressions of LGFs using Kummer's transformation can be found in Appendix B.

3. Numerical results

The computations for three LLNs and six typical LGFs are done using the method stated above for Earth models PREM, iasp91 and ak135, and their modified models in which the crustal physical parameters are given by the Crust 2.0 with soft and hard sediment as the outmost layer respectively. It is noted that the proposed variable transformation approach is used and has improved the stability of the numerical solutions of the ODEs. In order to assess the effect of this approach, we have done a comparison between two cases when the approach is used and not used. For the first case, the computation overflows when the degree is larger than 360 (or the resolution is less than 55 km), however, for the second case, the results are very stable for degrees up to 40,000, and validated by the asymptotic spherical solutions [Eq. (36) of Farrell, 1972] with the parameters of the top layers. The traditional Kummer's transformation (Farrell, 1972) used is found to be very important to speed up the converging of LGFs, and the disk factor technique (Farrell, 1972) is found to be necessary especially for the LGFs of tilt effect and radial strain component in the far field.

In this section, the results are shown and discussed for the three models in Section 3.1, and the modified models in Section 3.2.

3.1. PREM, iasp91 and ak135 Earth models

As seen in Fig. 1, the differences of physical parameters between iasp91 and ak135 are relatively small, however the differences between either one of these two and PREM are more significant in the crust, and especially in the 220 km discontinuity found by PREM. Such obvious differences in Earth structure can be reflected in the following computed LLNs (Fig. 3a–c) and LGFs (Fig. 4).

In order to easily find the gaps among the results of the three models, the percent differences are also computed between any two models of the three (iasp91 and PREM, ak135 and PREM, ak135 and iasp91). Only the relative differences for LLNs are shown in Fig. 3d–f, not shown for LGFs.

From Figs. 3 and 4 it is found that the differences of computed Load numbers and LGFs are not significant between ak135 and iasp91. The larger differences can be as large as ~3% for h_n ($n>200$), ~8% for l_n (n around 200), ~5.5% for k_n ($n>200$). For the computed six LGFs, the larger differences are mostly found for $\theta<10^\circ$. The relative differences are ~3% for radial displacement (u_r), ~10% for tangential displacement (v), ~0.2% for geoid anomaly(ΔN), ~2.0% for gravity change (g'), ~2.5% for tilt effect (t'), and ~14% for radial strain component ($e_{\theta\theta}$). The above differences should be caused by the discrepancies of physical parameters in the crust and the top of the mantle between the two Earth models.

As shown above, the results of computed LLNs and LGFs for iasp91 are very similar to those for ak135, thus in the following we just show the numerical features of the relative differences between ak135 and PREM by inspecting Figs. 3 and 4. For the three LLNs computed, there are larger differences between ak135 and PREM found for two ranges of degrees. For n around 200, the relative differences are ~14% for h_n, ~60% for l_n, 20% for k_n, and for $n>1000$, they are ~12% for h_n, ~3%

Table 1
Degree-one LLNs (h_1, l_1, k_1) for five different coordinate systems.

Earth model	Coordinate system	Degree-one LLNs		
		h_1	l_1	k_1
PREM	CE	−0.28430845	0.10304453	0
	CM	−1.2843084	−0.89695547	−1
	CF	−0.25823532	0.12911766	0.02607313
	CL	−0.38735298	0	−0.10304453
	CH	0	0.38735298	0.28430845
iasp91	CE	−0.28891623	0.10531330	0
	CM	−1.2889162	−0.89468670	−1
	CF	−0.26281969	0.13140984	0.02609654
	CL	−0.39422953	0	−0.10531330
	CH	0	0.39422953	0.28891623
ak135	CE	−0.28954527	0.10510547	0
	CM	−1.2895453	−0.89489453	−1
	CF	−0.26310049	0.13155025	0.02644478
	CL	−0.39465074	0	−0.10510547
	CH	0	0.39465074	0.28954527

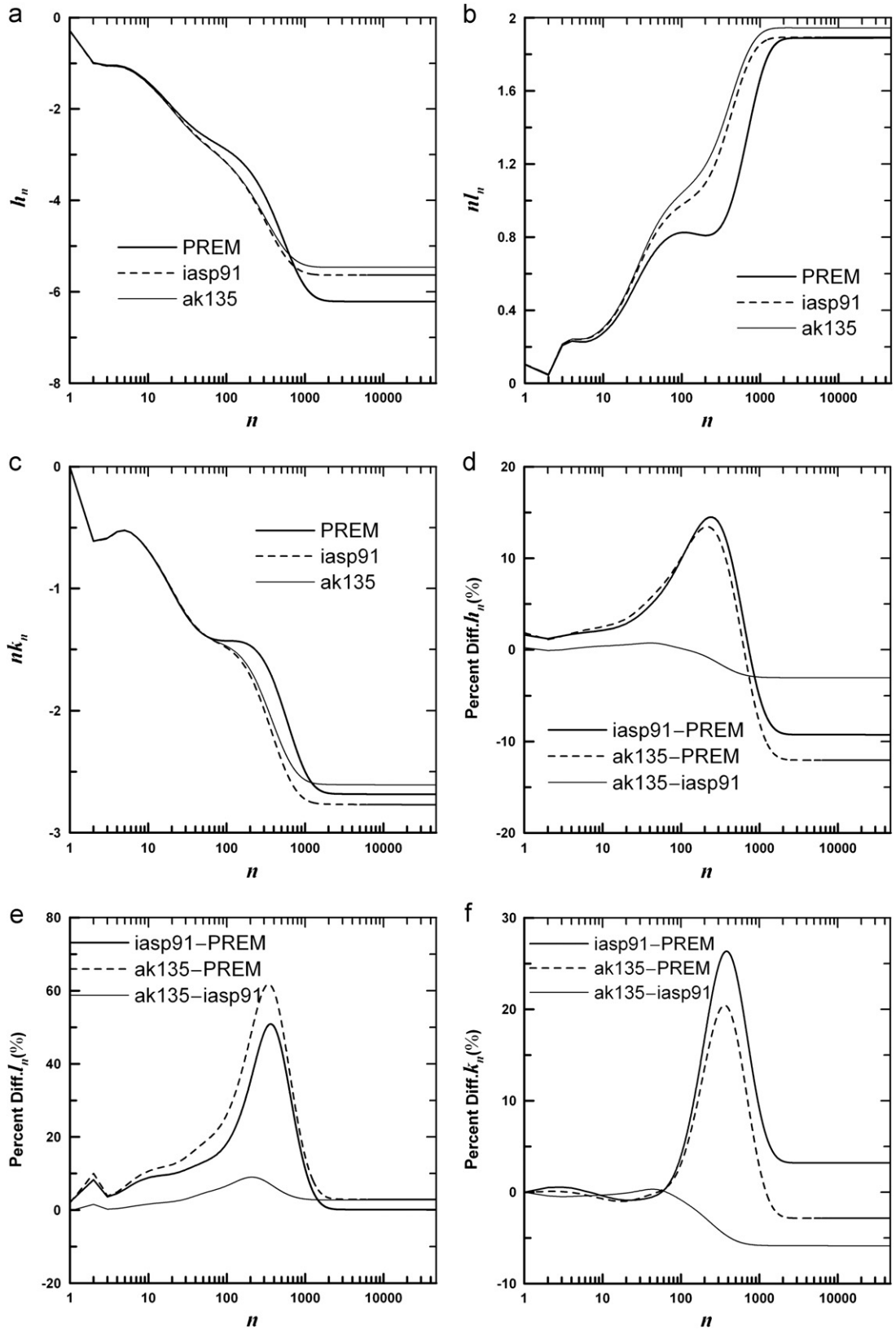

Fig. 3. LLNs (a–c) and their relative differences (d–f) computed for Earth models PREM, iasp91 and ak135. Note that 'iasp91–PREM' is the relative differences of results between iasp91 and PREM.

for l_n, 3% for k_n. For the six LGFs, larger differences are found for $\theta < 0.1^\circ$ with magnitudes of ~12% for u_r, ~3% for v, ~0.2% for ΔN, ~14% for g', ~10% for t', ~3.0% for $e_{\theta\theta}$, and also found for $0.1 < \theta < 1.0^\circ$ with larger magnitudes of ~26% for u_r, ~72% for v, ~0.2% for ΔN, ~25% for g', ~33% for t', and ~150% for $e_{\theta\theta}$. Note that for v and t', the larger differences extend to $\theta = 1.0^\circ$.

The above mentioned large differences of LLNs found for n around 200 and LGFs found $0.1 < \theta < 1.0^\circ$ between ak135

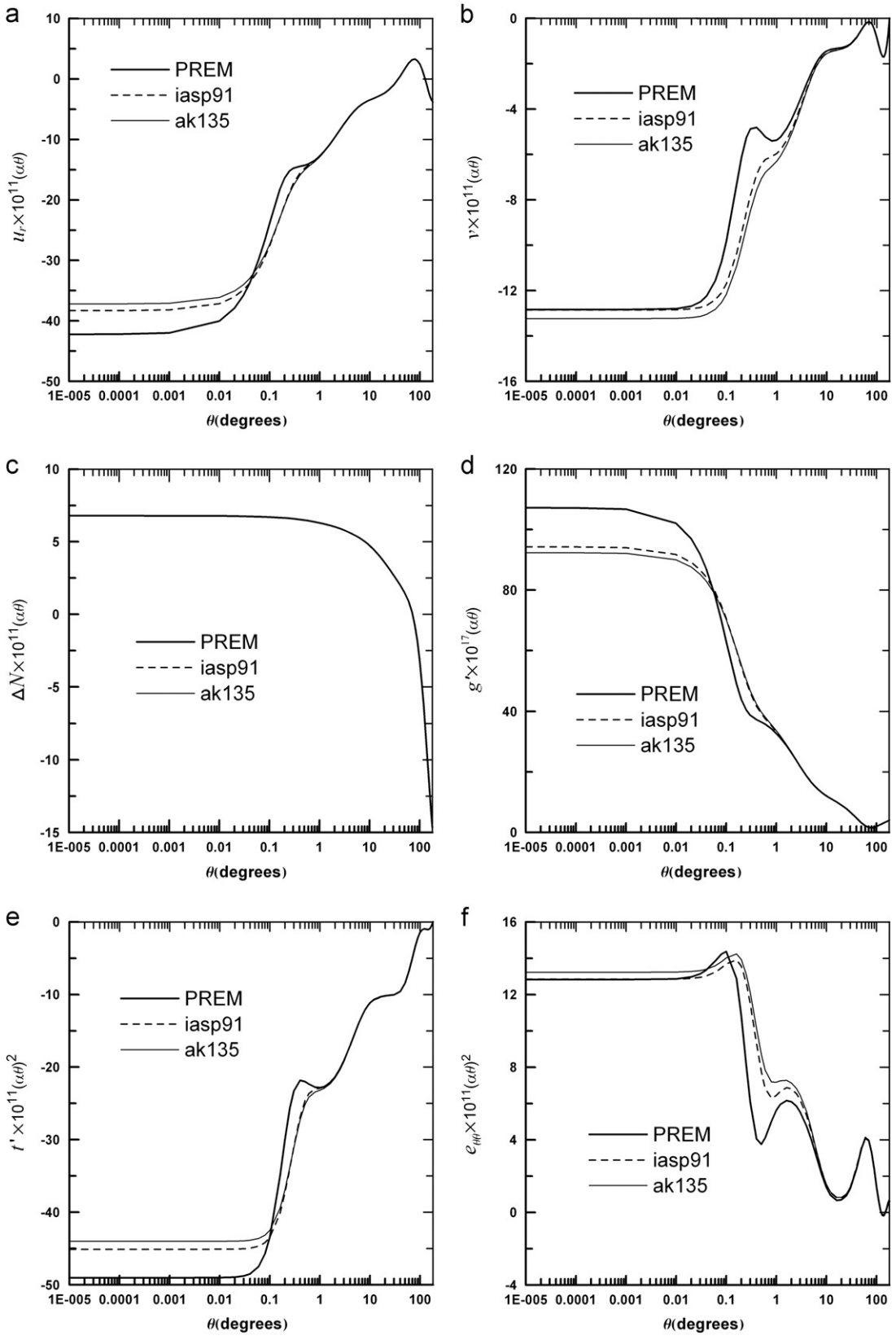

Fig. 4. LGFs computed for Earth models PREM, iasp91 and ak135. The units are arc for θ, t', cm for a, u_n, v and ΔN, cm s^{-2} for g', $e_{\theta\theta}$ is dimensionless. Mass of the applied load is 1 g.

and PREM may be induced by the 220 km discontinuity as occurred in the PREM model. However, the large differences of LLNs found in high degrees, and in LGFs for $\theta < 0.1^{\circ}$ may be resultant from the gaps of physical parameters of the two Earth models in the crust and the top of the mantle.

As shown above and also in Section 3.2, it is noted that results of the LGFs for ΔN are nearly not influenced by the selection of the Earth models in this paper. The reason is that they are mostly dependent upon the physical parameters of deeper Earth for which there are nearly no changes between any of the three Earth models to be compared.

3.2. 'Soft' and 'hard' Earth models

Inspection of Fig. 2 shows significant differences of physical parameters for depths within 20 km between Crust 2.0 and three Earth models PREM, iasp91 and ak135. This may change the results of LLNs for high degrees and LGFs in the near-field. In

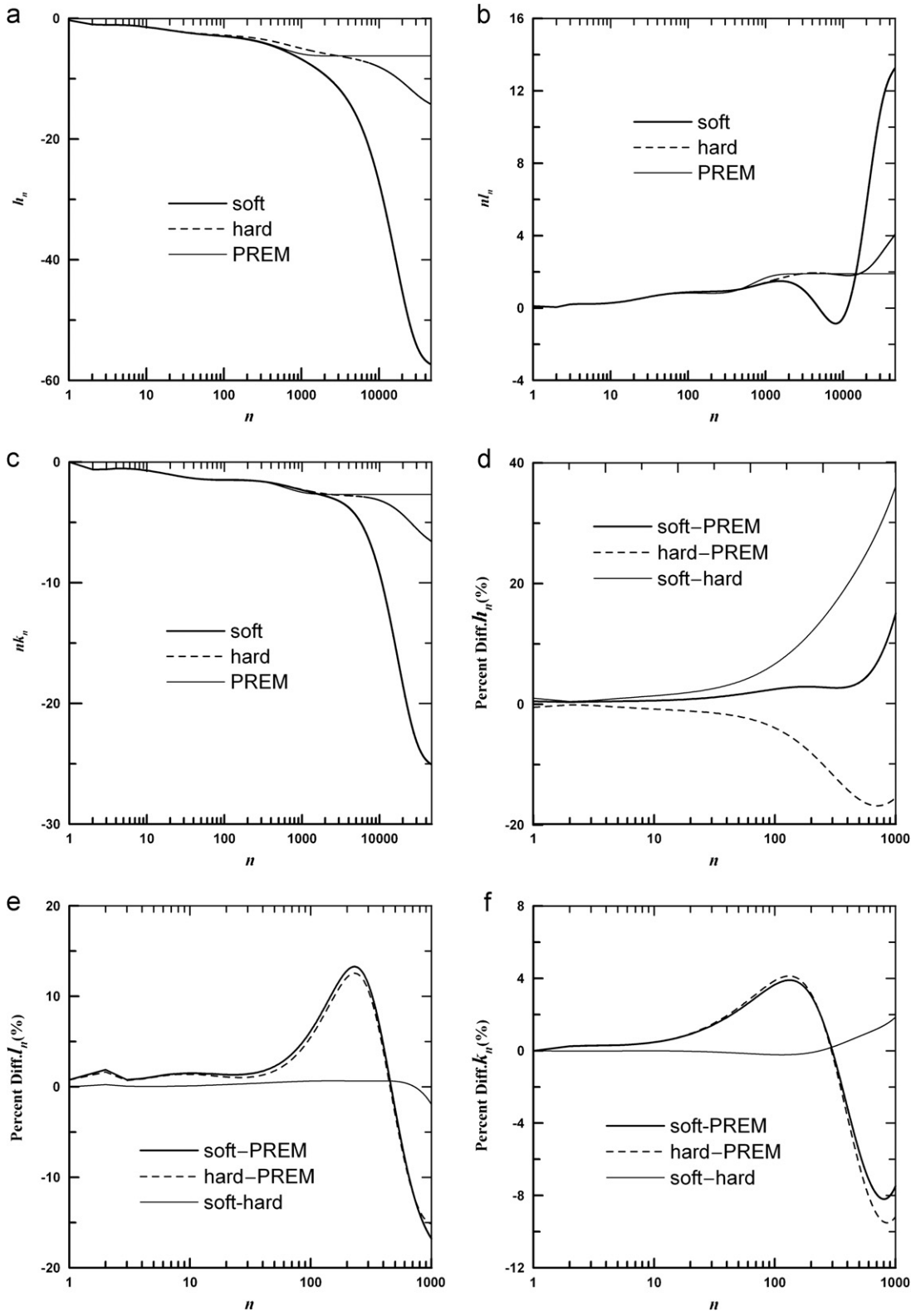

Fig. 5. LLNs (a–c) and their relative differences (d–f) computed for PREM and the two modified models 'soft' and 'hard' with crust replaced by Crust 2.0, with soft and hard sediment being outmost layers respectively.

order to investigate the effects of such differences, the crust structures of the above three Earth models are constituted by Crust 2.0 in which soft and hard sediments are considered as the outmost layers, then the relevant modified models are called as 'soft' and 'hard' models. Here, the LLNs and LGFs are computed for 'soft'/'hard' models of the above three models. The results, however, are shown only for the modified models of PREM and PREM itself for comparison in Figs. 5 and 6.

Based on the velocity values shown in Fig. 2, both the 'soft' and the 'hard' models of PREM have softer outmost layers than PREM

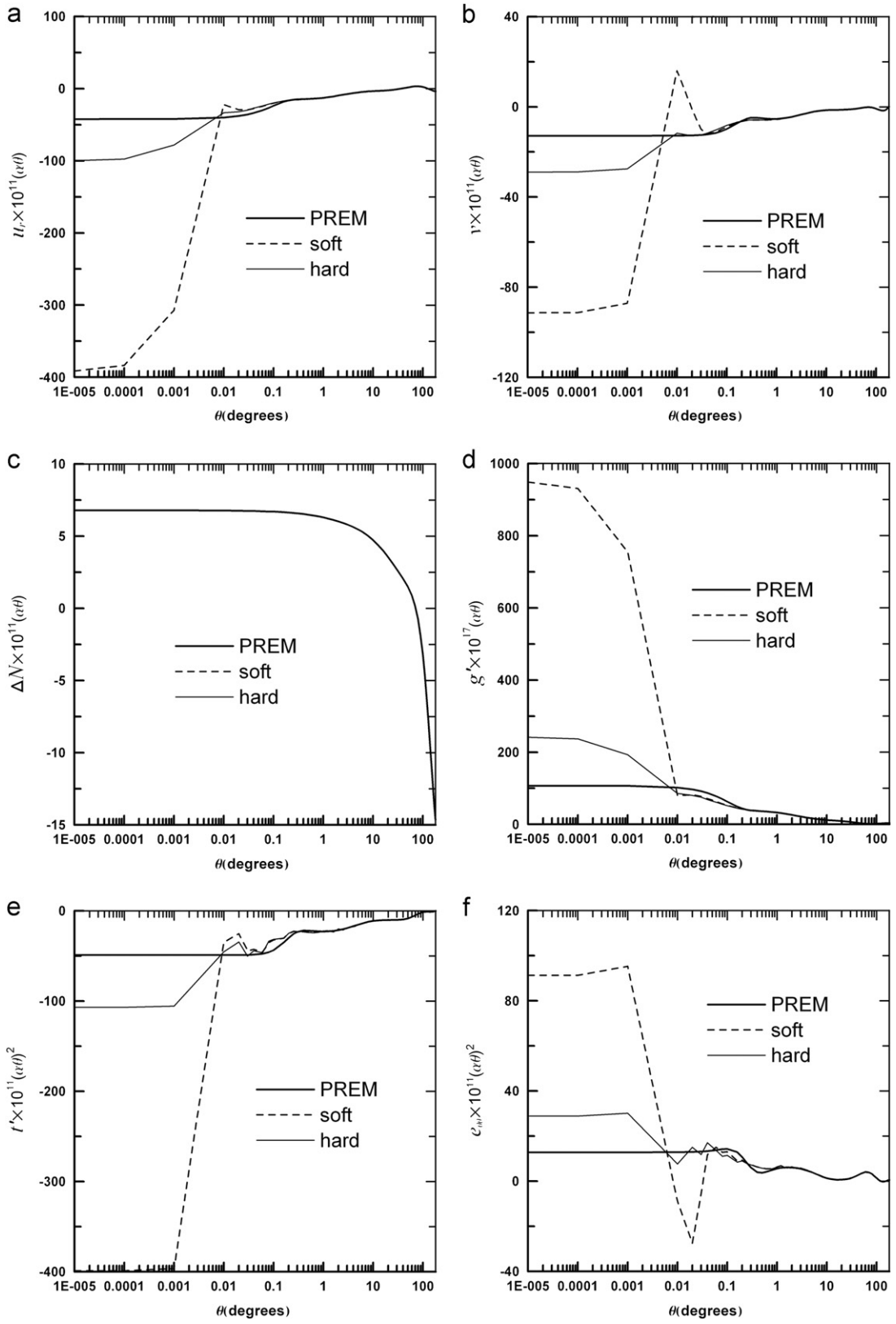

Fig. 6. LGFs computed for Earth models PREM, 'soft' and 'hard'. The units are arc for θ, t', cm for a, u_r, v and ΔN, cm s^{-2} for g', $e_{\theta\theta}$ is dimensionless. Mass of the applied load is 1 g.

while the top layer of 'soft' model is softer than 'hard' model. Such differences would influence the results of LLNs for high degrees and LGFs in the near-field except for geoid anomaly. From Fig. 5a–c and Fig. 6, large discrepancies of LLNs for high degrees (>1000) and LGFs in the regions ($<0.1^\circ$) are found between the 'hard' model and PREM, and even larger ones are found between the 'soft' model and PREM.

In addition, as seen in Fig. 2, the 'soft' and the 'hard' models have larger parameters from depth 10 km to 20 km than PREM. This causes certain differences of results of LLNs for degrees less than 1000 which cannot be easily seen in Fig. 5a–c. However, clear relative differences of results can be seen from Fig. 5d–f, the differences get large around degree 200 for l_{mn} and k_n while they have been increasing since tens of degrees for h_n. Taking $n=200$, the magnitudes of the relative differences between the 'hard' model and PREM are 8.1% for h_n, 12.1% for l_n and 3.1% for k_n; the differences between the 'soft' model and PREM are 3.0% for h_n, 12.8% for l_n and 3.0% for k_m. The differences between the 'soft' model and the 'hard' are 12.0% for h_n, 0.7% for l_n and 0.1% for k_n.

As shown in Sections 3.1 and 3.2, the differences of LLNs results for degrees up to several hundreds are worthy to be considered in the forward modeling for gravity changes from GRACE follow-on mission and the deformation from GPS assuming that they are caused by present-day surface mass transport (PDMT) or the inversion of PDMT using the data.

3.3. Data available and specifications

Results of LLNs and LGFs for the CE coordinate system (Farrell, 1972) are available for PREM, iasp91 and ak135 Earth models and their corresponding modified models PREMsoft/PREMhard, iasp91hard and ak135hard. PREMsoft and PREMhard are the modified models of PREM with soft and hard sediments as their outmost layers. Note that results for iasp91soft and ak135soft are not given since GPS sites are usually distributed in the hard rocks. The results for all the models are stored in directories 'LLNs' and 'LGFs' of directory 'loading data'.

Results of degree-one LLNs for other coordinate systems (CM, CF, CL and CH) can be calculated through Eqs. (20), (23)–(25) of Blewitt (2003) and are shown together with those for the CE coordinate system in Table 1. Note the results for the modified models are not shown since they are basically the same as those for PREM, iasp91 and ak135.

Results of LGFs for the four coordinate systems (CM, CF, CL and CH) are given by those for CE plus corrections of the corresponding degree-one terms (Blewitt, 2003). The corrections can be calculated following the expressions in Table B1 and the results are available in directory 'CORRs' of directory 'loading_data'. The specifications of all the data are included in file 'readme.txt'.

Note that the results of LGFs in Figs. 4 and 6 and in directory 'LGFs' and the degree one corrections in directory 'CORRs' have been normalized by factors $10^{11}(a\theta)$ for radial displacement (u_r), tangential displacement (v) and geoid anomaly (ΔN), $10^{17}(a\theta)$for gravity change (g^r), $10^{11}(a\theta)^2$ for tilt effect (t^r) and strain component ($e_{\theta\theta}$).

For strain components (B.6), the results are given only for component $e_{\theta\theta}$ while $e_{\lambda\lambda}$ and e_{rr} can be easily calculated with the results of u_r, v and $e_{\theta\theta}$.

3.4. M2 ocean tide loading effects at SHAO station

Here, in order to investigate how the loading effects in the near-field are affected by the uncertainty of the Earth model, we compute the M2 ocean tide loading effects for a coastal site—SHAO station, in Shanghai, China using the LGFs for the different Earth models in this paper. Data for M2 ocean tide are

Table 2
Results of M2 ocean tide loading in SHAO station (121.2°E, 31.27°N), Shanghai, China for different Earth models.

Earth model	Radial displacement		East displacement		North displacement		Gravity change		N–S tilt	
	A (mm)	α (deg.)	A (mm)	α (deg.)	A (mm)	α (deg.)	A (μgal)	α (deg.)	A (ms)	α (deg.)
ak135	7.642	−139.061	3.619	155.403	2.365	26.657	2.180	42.052	11.671	−37.824
iasp91	7.572	−139.634	3.546	155.658	2.278	24.108	2.164	41.680	11.610	−37.826
PREM	7.579	−139.884	3.252	156.359	2.060	19.645	2.147	40.588	10.833	−36.102
'hard'	7.580	−139.630	3.281	156.169	2.070	21.088	2.153	40.661	10.727	−35.494
'soft'	7.584	−139.616	3.288	156.149	2.079	21.372	2.153	40.687	10.762	−35.660

Earth model	E–W tilt		ε_{EE}		ε_{NN}		ε_{EN}		ε_{RR}	
	A (ms)	α (deg.)	A ($\times10^{-9}$)	α (deg.)	A ($\times10^{-9}$)	α (deg.)	A (ms)	α (deg.)	A ($\times10^{-9}$)	α (deg.)
ak135	17.910	−101.647	11.098	46.927	6.558	164.793	3.471	129.856	2.855	−97.251
iasp91	17.681	−101.719	9.913	44.017	6.119	166.039	3.318	130.228	2.777	−98.097
PREM	16.817	−103.814	7.667	27.512	4.453	179.311	2.644	132.580	1.682	−123.141
'hard'	17.064	−103.634	8.617	37.927	4.878	176.072	2.773	131.521	2.512	−108.927
'soft'	17.069	−103.554	8.696	38.094	4.924	175.466	2.792	131.482	3.244	−108.500

Note: A and α are the amplitude and phase for the computed quantities of the ocean tide loading; coordinate system used is CE; data for M2 ocean tide are given by DTU10 model (Cheng and Andersen, 2011). ε_{XY} denotes strain component with subscripts X, Y which can be eastern (E), northern (N) and radial (R) directions.

given by DTU10 model (Cheng and Andersen, 2011). The results are shown in Table 2.

It can be seen that the calculated differences for all the quantities between different Earth models are usually measurable except for the radial displacement. For the radial displacement, the differences of the amplitude are less than 0.l mm. However, for the two horizontal displacement components, the differences of the amplitude can be as large as 0.3–0.37 mm between PREM and ak135. For the gravity change, the differences of the amplitude are not large with magnitude of $\sim$33 μgal but still measurable using GWR gravimeter. For the two tilt components, the differences of the amplitude are as large as 1.0 ms. For the four strain components, the differences of the amplitude can be up to 3.3×10^{-9}, 2.1×10^{-9}, 0.9 ms, and 1.1×10^{-9}.

4. Conclusions and suggestions

LLNs and LGFs are computed for PREM, iasp91 and ak135 Earth models and for models with modified crust structure given by Crust 2.0. The differences of results among these models are carefully investigated in this paper.

Four conclusions can be made based on our investigation. First, the results of LLNs and LGFs are close between iasp91 and ak135, however they are quite different between either one of them and PREM for the LLNs for degrees around 200 and higher, and for LGFs when $0.1^\circ<\theta<1.0^\circ$as well as $\theta<0.1^\circ$. These may be caused by the effects of differences of elastic parameters at 220 km discontinuity and in the crust respectively. Second, due to softer crust, larger deformations are found for the modified models than the three models for the LLNs with degrees around 200 and high degrees, and LGFs in regions ($<0.1^\circ$). Third, there are no obvious changes found for the geoid anomaly when the three models are used or their crust structures are replaced by Crust 2.0. Fourth, for the most components of the M2 ocean tide loading, the differences of amplitude among the different Earth models used are large enough to be measured at SHAO station. This implies that the loading effects in the near-field computed may have larger uncertainties, and readers may use the LGFs for the different Earth models available in this paper to investigate the uncertainties of the loading effects in the near-field.

Therefore, our LGFs results suggest that iasp91 and ak135 should be considered in the modeling of the deformation fields within regions of colatitudes less than 1.0°, the crustal structure given by Crust 2.0 must be further used in the regions ($<0.1^\circ$). In addition, our LLN results of multiple models with degrees up to several hundreds available in this paper can be used for forward modeling of the GRACE gravity changes and GPS deformations resulting from surface mass transport (e.g., polar ice-melting, land water/ice/snow storage changes) or for the inversion of surface mass transport using the two types of data respectively.

Acknowledgments

H. Wang is supported by the National Natural Science Foundation of China (Grant nos. 40825012, 41021003, and 41174016), the National key Basic Research Program of China (973 Program) (Grant no. 2012CB957703) and the CAS/SAFEA International Partnership Program for Creative Research Teams (Grant no. KZZD-EW-TZ-05). L. Jiang is supported by the Hundred Talents Program of the Chinese Academy of Sciences, and the National Key Technology Research and Development Program of the Ministry of Science and Technology of China (no. 2011BAK12B02). We thank Dr. Yongcun Cheng from Technical University of Denmark for providing us their new global ocean tide model DTU10.

Appendix A. Computation of LLNs

For $n>1$, LLNs

$$\begin{bmatrix} h_n \\ l_n \\ k_n+1 \end{bmatrix} = \frac{g_0(a)}{\Phi_{2n}(a)} \begin{bmatrix} y_{11}(a) & y_{12}(a) & y_{13}(a) \\ y_{21}(a) & y_{22}(a) & y_{23}(a) \\ -y_{51}(a)/g_0 & -y_{52}(a)/g_0 & -y_{53}(a)/g_0 \end{bmatrix} \times \begin{bmatrix} y_{31}(a) & y_{32}(a) & y_{33}(a) \\ y_{41}(a) & y_{42}(a) & y_{43}(a) \\ y_{61}(a) & y_{62}(a) & y_{63}(a) \end{bmatrix}^{-1} \begin{bmatrix} y_3(a) \\ y_4(a) \\ y_6(a) \end{bmatrix}, \quad n>1, \tag{A.1}$$

in which, $\Phi_{2n}(a)=ag_0(a)/m_e$.

For $n=1$, LLNs are given respectively for different coordinate systems (Farrell, 1972; Blewitt, 2003).

For CE coordinate system, it is chosen where the origin always coincides with the center of mass of the solid Earth, the degree one LLNs are calculated by:

$$\begin{bmatrix} h_1 \\ l_1 \\ k_1 \end{bmatrix}_{\mathrm{CE}} = \begin{bmatrix} h_1^c-k_1^c \\ l_1^c-k_1^c \\ 0 \end{bmatrix}, \tag{A.2}$$

in which,

$$\begin{bmatrix} h_1^c \\ l_1^c \\ k_1^c+1 \end{bmatrix} = \frac{g_0(a)}{\Phi_{21}(a)} \begin{bmatrix} y_{11}(a) & y_{12}(a) \\ y_{21}(a) & y_{22}(a) \\ -y_{51}(a)/g_0 & -y_{52}(a)/g_0 \end{bmatrix} \times \begin{bmatrix} y_{31}(a) & y_{32}(a) \\ y_{41}(a) & y_{42}(a) \end{bmatrix}^{-1} \begin{bmatrix} y_3(a) \\ y_4(a) \end{bmatrix}, n=1 \tag{A.3}$$

In Eqs. (A.1) and (A.3), $\left(y_{1j}(a),y_{2j}(a),y_{3j}(a),y_{4j}(a),y_{5j}(a),y_{6j}(a)\right)^t$ ($j=1,2,3$) is the result of integrating ODEs (Eq. (8) of Wu and Peltier, 1982) on the Earth surface from the initial value for the jth vector of (Eq. (48) of Wu and Peltier, 1982) at the CMB using the Runge–Kutta method.

For other coordinate systems (CM, CF, CL and CH), the degree one LLNs can be simply calculated using Eq. (A.2), the formulas are not shown here and can be found in Eqs. (20) and (23)–(25) of Blewitt (2003).

Appendix B. Expressions of LGFs using Kummer's transformation

The expressions of LGFs for the six representative observables are given below by using Kummer's transformation

Radial displacement

$$u_r(\theta)=\frac{ah_\infty}{m_e}\left(\frac{1}{2\alpha_s}-1\right)+\frac{a}{m_e}\sum_{n=1}^{\infty}(h_n-h_\infty)P_n(\cos\theta) \tag{B.1}$$

Tangential displacement

$$v(\theta)=-\frac{al_\infty\alpha_c(1+2\alpha_s)}{2m_e\alpha_s(1+\alpha_s)}+\frac{a}{m_e}\sum_{n=1}^{\infty}\frac{nl_n-l_\infty}{n}\frac{\partial P_n(\cos\theta)}{\partial\theta} \tag{B.2}$$

Geoid anomaly

$$\Delta N(\theta)=\frac{a}{m_e}\left[\frac{1}{2\alpha_s}-1-k_\infty\ln(\alpha_s+\alpha_s^2)\right]+\frac{a}{m_e}\sum_{n=1}^{\infty}\frac{nk_n-k_\infty}{n}P_n(\cos\theta) \tag{B.3}$$

Gravity change

$$g'(\theta)=-\frac{g_0(a)}{m_e}\left\{(2h_\infty-k_\infty)\left(\frac{1}{2\alpha_s}-1\right)-\frac{1}{4\alpha_s}+k_\infty\ln(\alpha_s+\alpha_s^2)\right\} -\frac{g_0(a)}{m_e}\sum_{n=1}^{\infty}\left[2(h_n-h_\infty)-\frac{(n+1)(nk_n-k_\infty)}{n}\right]P_n(\cos\theta) \tag{B.4}$$

Table B1
Degree one corrections for the three LGFs with respect to CE coordinate system.

Coordinate systems	Degree one corrections for the three LGFs		
	$u_r(\theta)$	$v(\theta)$	$\Delta N(\theta)$
CM	$-\frac{a}{m_e}\cos\theta$	$\frac{a}{m_e}\sin\theta$	$-\frac{a}{m_e}\cos\theta$
CF	$-\frac{h_1+2l_1}{3}\frac{a}{m_e}\cos\theta$	$\frac{h_1+2l_1}{3}\frac{a}{m_e}\sin\theta$	$-\frac{h_1+2l_1}{3}\frac{a}{m_e}\cos\theta$
CL	$-\frac{a}{m_e}l_1\cos\theta$	$\frac{a}{m_e}l_1\sin\theta$	$-\frac{a}{m_e}l_1\cos\theta$
CH	$-\frac{a}{m_e}h_1\cos\theta$	$\frac{a}{m_e}h_1\sin\theta$	$-\frac{a}{m_e}h_1\cos\theta$

Note: (h_1, l_1, k_1) are the degree one LLNs for CE coordinate system given by (A.2).

Tilt effect

$$t'(\theta)=\frac{1}{m_e}\left[\frac{(h_\infty-1)\alpha_c}{4\alpha_s^2}-\frac{k_\infty\alpha_c(1+\alpha_s)}{2\alpha_s(1+\alpha_s)}\right]+\frac{1}{m_e}\sum_{n=1}^{\infty}\left[h_\infty-h_n+\frac{nk_n-k_\infty}{n}\right]\frac{\partial P_n(\cos\theta)}{\partial\theta} \tag{B.5}$$

Strain components

$$\begin{cases} e_{\theta\theta}(\theta)=\frac{u_r(\theta)}{a}+\frac{l_\infty(1+\alpha_s+\alpha_s^2)}{4m_e\alpha_s^2(1+\alpha_s)}+\frac{1}{m_e}\sum_{n=1}^{\infty}\frac{nl_n-l_\infty}{n}\frac{\partial^2 P_n(\cos\theta)}{\partial\theta^2} \\ e_{\lambda\lambda}(\theta)=\frac{u_r(\theta)}{a}+\cot\theta\frac{v(\theta)}{a} \\ e_{r\theta}(\theta)=0 \\ e_{rr}(\theta)=-\frac{\lambda(a)}{\lambda(a)+2\mu(a)}\left[e_{\theta\theta}(\theta)+e_{\lambda\lambda}(\theta)\right],\quad \theta>0 \end{cases} \tag{B.6}$$

In Eqs. (B.1)–(B.6), $\alpha_s=\sin(\theta/2)$, $\alpha_c=\cos(\theta/2)$. The degree zero terms are not included for radial displacement (B.1), geoid anomaly (B.3) and gravity change (B.4) due to load mass conservation.

Radial displacement (B.1), tangential displacement (B.2) and geoid anomaly (B.3) can be different for different coordinates systems due to the differences of degree one term. For the coordinate systems CM, CF, CL and CH, the differences are given with respect to CE system for the three quantities in Table B1.

Appendix C. Supporting information

Supplementary data associated with this article can be found in the online version at http://dx.doi.org/10.1016/j.cageo.2012.06.022.

References

Blewitt, G., 2003. Self-consistency in reference frames, geocenter definition, and surface loading of the solid Earth. Journal of Geophysical Research 108 (B2), 2103.

Cheng, Y., Andersen, O.B., 2011. Multimission empirical ocean tide modeling for shallow waters and polar seas. Journal of Geophysical Research 116, C11001.

Dziewonski, A.M., Anderson, D.L., 1981. Preliminary reference Earth model. Physics of the Earth and Planetary Interiors 25, 297–356.

Farrell, W.E., 1972. Deformation of the Earth by surface loads. Review of Geophysics and Space Physics 10 (3), 761–797.

Guo, J.-Y., Ning, J.-S., Zhang, F.-P., 2001. Chebyshev-collocation method applied to solve ODEs in geophysics singular at the Earth center. Geophysical Research Letters 28 (15), 3027–3030.

Han, D., Wahr, J., 1995. The viscoelastic relaxation of a realistically stratified Earth, and a further analysis of postglacial rebound. Geophysical Journal International 120, 287–311.

Kennett, B.L.N., Engdahl, E.R., 1991. Travel times for global earthquake location and phase identification. Geophysical Journal International 105, 429–465.

Kennett, B.L.N., Engdahl, E.R., Buland, R., 1995. Constraints on seismic velocities in the Earth from travel times. Geophysical Journal International 122, 108–124.

Laske, G., Masters, G., Reif, C., 2012. CRUST 2.0: A New Global Crustal Model at 2×2 Degrees. ⟨http://igppweb.ucsd.edu/~gabi/crust2.html⟩.

Longman, I.M., 1963. A Green's function for determining the deformation of the Earth under surface mass loads, 2. Computation and numerical results. Journal of Geophysical Research 68, 485–496.

Longman, I.M., 1962. A Green's function for determing the deformation of the Earth under surface mass loads, 1. Theory. Journal of Geophysical Research 67, 845–850.

Na, S.-H., Baek, J., 2011. Computation of the Load Love number and the Load Green's function for an elastic and spherically symmetric earth. Journal of the Korean Physical Society 58 (5), 1195–1205.

Pagiatakis, S.D., 1990. The response of a realistic earth to ocean tide loading. Geophysical Journal International 103 (2), 541–560.

Peltier, W.R., Andrews, J.T., 1976. Glacial isostatic adjustment I: the forward problem. Geophysical Journal of the Royal Astronomical Society 46, 605–646.

Plag, H.-P., Juitner, H.-U., Rautenberg, V., 1996. On the possibilty of global and regional inversion of exogenic deformations for mechanical properties of the Earth's interior. Journal of Geodynamics 21 (3), 87–308.

Riva, R.E.M., Vermeersen, L.L.A., 2002. Approximation method for high-degree harmonics in normal mode modeling. Geophysical Journal International 151, 309–313.

Van Dam, T., Plag, H.-P., Francis, O., Gegout, P., 2002. GGFC special bureau for loading: current status and plans. IERS Technical Note 30, 180–198.

Wang, H., Hsu, H., Li, G., 1996. Improvement of computations of load Love numbers of SNREI Earth model. Chinese Journal of Geophysics 39 (Suppl), 182–189.

Wang, R., Wang, H., 2007. A fast converging and anti-aliasing algorithm for Green's functions in terms of spherical or cylindrical harmonics. Geophysical Journal International 170, 239–248.

Wu, P., Peltier, W.R., 1982. Viscous gravitational relaxation. Geophysical Journal of the Royal Astronomical Society 70, 435–485.